Original Research Article: full paper

(2023), «EUREKA: Physics and Engineering»
Number 6

CALIBRATING POLYPROPYLENE PARTICLE MODEL PARAMETERS WITH UPSCALING AND REPOSE SURFACE METHOD

Supattarachai Sudsawat
Department of Materials Handling and Logistics Engineering[1]

Pornchai Chongchitpaisan
Department of Materials Handling and Logistics Engineering[1]

Pirapat Arunyanart✉
Department of Materials Handling and Logistics Engineering[1]
pirapat.a@eng.kmutnb.ac.th

[1]*King Mongkut's University of Technology North Bangkok*
1518 Pracharat 1 Road, Wongsawang, Bangsue, Bangkok, Thailand, 10800

✉**Corresponding author**

Abstract

The discrete element method (DEM) is a computational technique extensively utilized for simulating particles on a large scale, specifically focusing on granular materials. Nonetheless, its implementation requires a substantial amount of computational power and accurate material properties. Consequently, this study delves into an alternative approach referred to as volume-based scaled-up modeling, aiming to simulate polypropylene particles using DEM while mitigating the computational burden and regenerating new material properties. This novel method aims to reduce the CPU time required for the simulation process and represent both the macro mechanical behavior and micro material properties of polypropylene particles. To accomplish this, the dimensions of the polypropylene particles in the DEM simulation were magnified by a factor of two compared to the original size of the prolate spheroid particles. In order to determine the virtual micro material properties of the polypropylene particles, a calibration method incorporating the design of experiments (DOE) and repose surface methodology was employed. The predicted bulk angle of repose (AOR) derived from the upscaled DEM parameters exhibited a remarkably close agreement with the empirical AOR test, demonstrating a small relative error of merely 1.69 %. Moreover, the CPU time required for the upscaled particle model proved to be less than 71 % of that necessary for the actual-scale model of polypropylene particles. These compelling results confirm the effectiveness of enlarging the particle volume used to calibrate micro-material properties in the Discrete Element Method (DEM) through the DOE technique. This approach proves to be a reliable and efficient method.

Keywords: DEM, design of experiments, volume-based scaled-up modeling, CPU time, AOR.

DOI: 10.21303/2461-4262.2023.002968

1. Introduction

The discrete element method (DEM) was introduced [1] as a valuable tool for simulating particle handling across industries such as mining, agriculture, geotechnical applications, and polymer processing [2–7]. DEM enables prediction of dynamic behavior, design optimization, and validation of virtual models for materials handling [8]. As granular material handling challenges are significant due to their prevalence in storage (over 40 %), accurate input parameters for material properties are crucial [9]. A robust calibration methodology is necessary, considering both macro and micro properties, to derive efficient parameters from experimental and numerical tests [10–12]. Parameters related to particle shape, material properties, optimization, and scaling play a vital role in effective calibration of bulk material parameters in DEM [10].

Several studies have contributed to the calibration of the discrete element method (DEM). The study [10] used shear box, angle of repose, and hopper discharge experiments to calibrate particle stiffness and friction coefficient in crushed rock particles. The researchers analyzed the behavior of spherical and convex particles, specifically looking at how the angle of repose is affected by factors such as the number of particles and the friction coefficients [13]. The paper [14]

investigated iron ore particles, considering sliding and rolling friction coefficients and particle size. The simulations conducted by the researchers demonstrated a high level of concurrence with experimental results for alumina pellets, lunar soil particles, and wet coal particles, respectively [15–17]. Other researchers [18–20] emphasized the importance of sliding and rolling friction coefficients and cohesion energy density for cohesive and cohesionless bulk materials. Free-flow tests were found to provide more accurate angle of repose determination compared to lifting cylinder and shear box tests [21, 22]. Research groups have used genetic algorithms, neural network algorithms, and surrogate modeling-based calibration to optimize DEM parameters [23–29]. Scaling up bulk particle research reduces computational time while maintaining macroscopic behavior and mechanical properties [30–32]. Scaling corn particles [31] improved agreement between DEM simulations and experiments.

No previous studies were found on scale-up DEM modeling specifically for polypropylene (PP) particles, despite their widespread use and significance in the global plastics market [33]. This research focuses on investigating the scaled-up DEM model for PP material properties for reducing CPU time through calibration based on the angle of repose. Image processing techniques will validate the angle of repose for both DEM simulations and physical experiments. Micro material parameters will be optimized using DOE, response surface methodology, and exact optimization methods.

2. Materials and methods

2. 1. Polypropylene grain material properties

The spherical polypropylene particles (**Fig. 1**) were utilized. Their dimensions were measured using a digital Vernier caliper, with 100 random samples taken. Particle mass was determined by weighing 200 polypropylene particles on a precise digital scale [8]. The density of polypropylene was measured following ASTM guidelines [34]. Bulk density was obtained through a laboratory test involving a cup and a filling funnel, with repeated weightings after filling the cup [8]. Bulk density was calculated using (1) [35]:

$$\rho_b = \frac{M_{pc} - M_c}{V}, \tag{1}$$

where, ρ_b is the bulk density, M_{pc} is the mass of the polypropylene grains filled cup, M_c is the mass of the empty cup, and V is the inner volume of the cup.

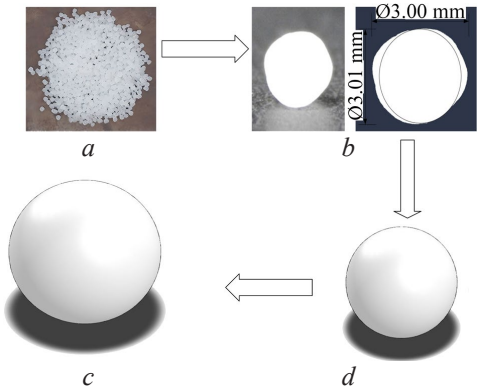

Fig. 1. A polypropylene particle: *a* – an actual particle sample; *b* – its equivalent dimensions; *c* – a simplified spheroid particle; *d* – a scaled-up DEM polypropylene particle

2. 2. Coarse graining technique

The concept of upscaling particle methodology is introduced, suggesting that a system with larger grain dimensions can maintain an equivalent energy density to that of the original particle sizes [36]. In this methodology, the volume fraction and particle density should remain unchanged, as described in (2), where ρ_{actual} and ρ_c represents the density of original and upscaled particles.

(3) presents the scaling factor (s) for the relationship between the radius of the original particles (r) and the coarser particles (r'), assuming they have spherical shapes. In this research, a scaling factor of 2 will be applied [30, 32]:

$$\rho_{actual} = \rho_c, \tag{2}$$

$$r' = sr. \tag{3}$$

Accordingly, the mass and the moment of inertia (I) of the up-scaled particles can provide according to (4) and (5) respectively:

$$m' = \frac{4}{3}\pi r'^3 \rho_c = s^3 m, \tag{4}$$

$$I' = \frac{2}{3} m' r'^2 = s^5 I. \tag{5}$$

The equivalent mass (m') is defined as the original particle mass (m), and the actual mass is denoted as m. The study [36] suggests that the kinetic energy can be derived by assuming that coarse grains exhibit similar kinetic energy behavior as indicated in (6):

$$\frac{1}{2} m' v'^2 = s^3 \frac{1}{2} m v^2. \tag{6}$$

This research necessitates precise scaling of stiffness and damping values in (7)–(10) for the Hertz-Mindlin contact model:

$$F_n = F_{k,n} + F_{d,n} = k_n \delta_n^{\frac{3}{2}} i_n + c_n v_n \sqrt{\frac{3}{2} k_n \delta_n^{\frac{1}{4}}}, \tag{7}$$

$$F_t = F_{k,t} + F_{d,t} = k_t \sqrt{\delta_n \delta_t}\, i_t + c_t v_t \sqrt{k_t \delta_n^{\frac{1}{4}}}, \tag{8}$$

$$k_n = \frac{4}{3} E^* \sqrt{r'} \text{ and } c_n = -2\sqrt{\frac{5}{6}} \beta \sqrt{m'}, \tag{9}$$

$$k_t = -8 G^* \sqrt{r'} \text{ and } c_t = -2\sqrt{\frac{5}{6}} \beta \sqrt{m'}. \tag{10}$$

k_n and c_n represent normal stiffness and damping coefficients, while k_t and c_t denote tangential counterparts. δ_n and δ_t refer to normal and tangential overlaps, and i_n and i_t represent normal and tangential unit vectors. E^*, G^* and β represent equivalent Young's modulus, shear modulus, and coefficient of restitution.

Fig. 2 shows the spring and damper systems for both the original four particles and the coarse grain particle ($s = 2$) [32]. The stiffness (k_n') and damping (c_n') of the coarse grain particles should match the equivalent stiffness (k_e) and damping (c_e) of the cluster of original four particles. (11) derives the relationship between the equivalent stiffness and the stiffness of the original particles:

$$k_e = s^2 k_{series} = s^2 \frac{\frac{1}{2} F_k}{\delta_{series}^{1.5}} = s^2 \frac{\frac{1}{2} F_k}{(s\delta_n)^{1.5}} = s^2 \frac{\frac{F_{k,series}}{\delta_n^{1.5}}}{s^{1.5}} = s^2 \frac{k_n}{s^{1.5}} = \sqrt{s} k_n. \tag{11}$$

From Equation (9) of the Hertz-Mindlin model, the stiffness contact between the coarse and original systems can be expressed as Equation (12), where k_{series} represents the stiffness of each of the two pairs and the mechanical properties, like Young's modulus (E), are preserved in the coarse system:

$$k_n' = \frac{4}{3} E'^* \sqrt{r'^*} = \sqrt{s} \frac{4}{3} E' \sqrt{r^*} = \sqrt{s} k_n = k_e. \tag{12}$$

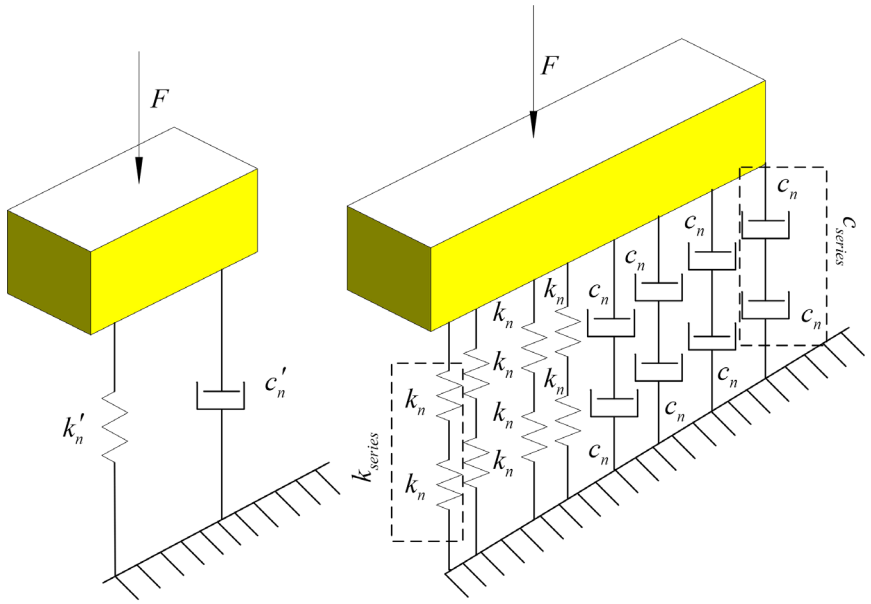

Fig. 2. The contact model: *a* – the up-scaled coarse grain particles; *b* – the equivalent actual particles

The tangential stiffness (k_t) will be scaled according to (10), while the equivalent damping stiffness (c_e) can be obtained by applying a scaling factor of s^2 to the damping series of the original system (c_{series}), as shown in (13):

$$c_e = s^2 c_{series} = s^2 \frac{\frac{1}{2}F_c}{v_{series}\sqrt{k_{series}\delta_{series}^{1.5}}} = s^2 \frac{\frac{1}{2}F_c}{v_n\sqrt{\frac{k_n}{s^{1.5}}(s\delta_n)^{1.5}}} =$$

$$= s^2 \frac{\frac{1}{2}F_c}{\sqrt{s}v_n\sqrt{k_n(\delta_n)^{1.5}}} = s^2 \frac{\frac{F_{c,series}}{v_n\sqrt{k_n(\delta_n)^{1.5}}}}{\sqrt{s}} = s^2 \frac{c_n}{\sqrt{s}} = s^{1.5}c_n. \quad (13)$$

(11) with $\delta_{series} = s\delta_n$ and equal velocities (v_n) for both upscaled and original particles implies that (9) yields the corresponding normal damping coefficient Equation (14), while the tangential damping coefficient remains the same as (10):

$$c_n' = 2\sqrt{\frac{5}{6}}\beta\sqrt{m'^*} = s^{1.5}2\sqrt{\frac{5}{6}}\beta\sqrt{m'^*} = s^{1.5}c_n = c_e. \quad (14)$$

The normal contact force in upscaled materials is s^3 times that of the actual particle system [37]. Consequently, the relationship between tangential (F_t) and normal (F_n) forces will also be s^3 times for upscaled particles. This scaling factor applies to the kinetic rotational energy of the coarse-grained system, as demonstrated in (15), (16):

$$F_t' = \mu_s F_n' = \mu_s s^3 F_n, \quad (15)$$

$$\frac{1}{2}I'\dot{\theta}'^2 = s^3\frac{1}{2}I\dot{\theta}^2. \quad (16)$$

μ_s represents the static friction coefficient and $\dot{\theta}$ denotes the rotational velocity. All formulas show the equivalent properties between coarse and actual systems.

2. 3. Scaled-up polypropylene particle and fixed funnel equipment establish

Fig. 3, *b* demonstrates DEM simulation tests aiming to replicate fixed funnel laboratory tests on a real scale, with particles poured from a funnel, forming a heap in a cup (**Fig. 3, *a, b***). The angle of repose was determined using image analysis and the inverse tangent rule [30, 32].

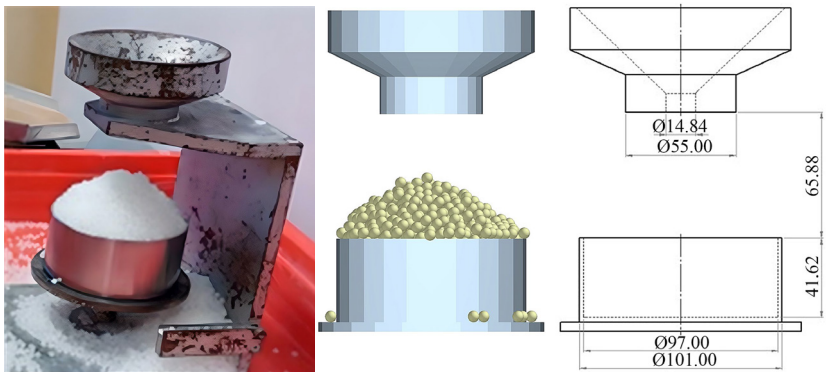

a *b*

Fig. 3. Fixed funnel: *a* – experimental test; *b* – Discrete Element Method simulation

2. 4. Discrete Element Method material constitution

The EDEM software simulated the angle of repose using the fixed funnel method and shear box test. The Hertz Mindlin model calculated particle geometry and interactions, while (6), (7) determined the forces. Constitutive equations were derived using Coarse graining. **Table 1** provided initial values for the DEM PP particle. Simulation settings included a Rayleigh Time step, 20 s total simulation time, and a save interval of 0.02s. The computer had 12-core processors, 3.7 GHz, and 16 GB RAM.

Table 1

Initial DEM material properties estimation

Material type	Parameters	Values	Sources
Material Properties			
Polypropylene (PP)	Poisson's ratio	0.36, 0.41	c, g
	Solid density (kg·m^{-3})	889, 910, 1107	b, g, a
	Elastic modulus (GPa)	1.3, 1.9, 2	e, f, c
Steel	Poisson's ratio	0.3	c
	Solid density (kg·m^{-3})	7800	d
	Elastic modulus (GPa)	198	c
Interaction parameters			
Coefficient of static friction	PP-PP	0.1, 0.153, 0.22, 0.3, 0.6	a, g, j, b, d
	PP-Steel	0.26, 0.3	j, d, e
Coefficient of dynamic friction	PP-PP	0.05, 0.44	g, e
	PP-Steel	0.246, 0.28	j, e
Coefficient of restitution	PP-PP	0.3, 0.49, 0.9, 0.97	d, g, b, a
	PP-Steel	0.55, 0.71	j, e

Source: a – 38; b – 39; c – 40; d – 41; e – 42; f – 43; g – 7; j – experiment results

2. 5. Indirect measurement of angle of repose

Fig. 4 presents an algorithm for determining the angle of repose. The algorithm involves selecting the appropriate area, creating binary images, filtering out noise, mapping pixel coordinates to *x* and *y* axes, and plotting pixel values. The resulting arched figure in **Fig. 4** is used to estimate the angle of repose through linear regression using the least square method.

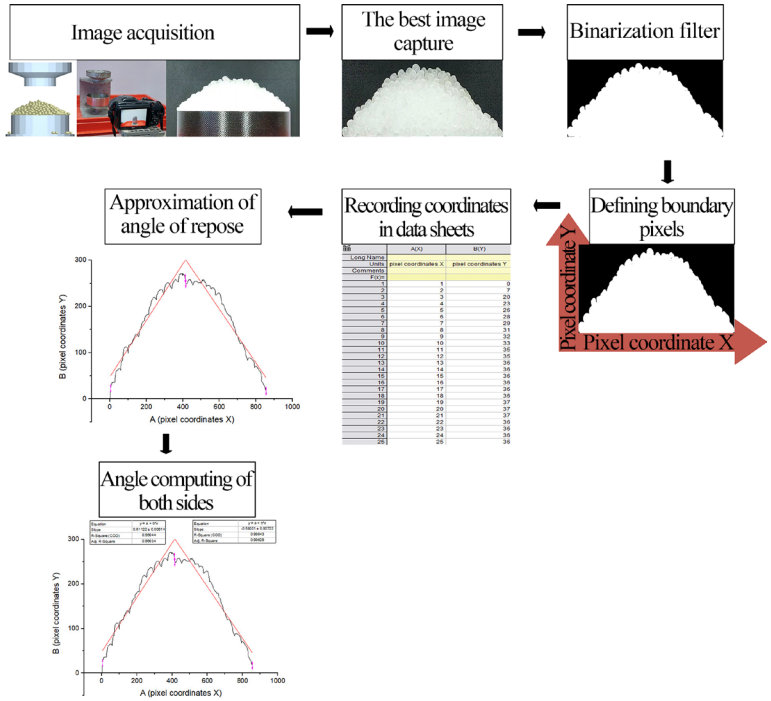

Fig. 4. The algorithm of angle of repose procedure both experiment and Discrete Element Method simulation tests

2. 6. The research methodology

Fig. 5 illustrates the flowchart of the methodology, which includes gathering micro parameters, screening important parameters, designing experiments, creating an angle of repose model, finding optimal values, performing DEM simulation, comparing with empirical test, and obtaining suitable micro parameters for Upscaling DEM Model.

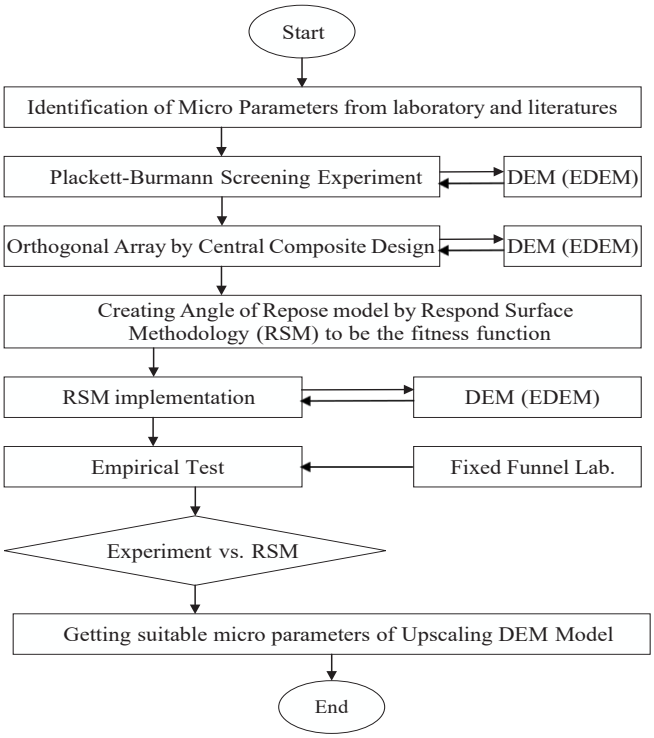

Fig. 5. Flow chart of methodology

Both empirical and simulation-based Angle of Repose (AOR) tests were conducted using an indirect measurement method employing image processing techniques.

2. 6. 1. Identification of micro parameter for upscaling DEM model

Relevant parameters were collected from previous research papers and laboratory tests [38–44]. The initial analysis used fractional two-level factors, with the parameter ranges shown in **Table 2**.

Table 2
Micro parameters and levels

Screening Experiment (Unit)	Symbol	Level	
		Low	High
1. Poisson's ratio (PP)	*A*	0.36	0.41
2. Solid density(kg/m^3) (PP)	*B*	889	1107
3. Elastic modulus (GPa) (PP)	*C*	1.3	2
4. Coefficient of restitution (PP-PP)	*D*	0.30	0.97
5. Coefficient of restitution (PP-Steel)	*E*	0.55	0.71
6. Coefficient of static friction (PP-PP)	*F*	0.1	0.6
7. Coefficient of static friction (PP-Steel)	*G*	0.26	0.3
8. Coefficient of dynamic friction (PP-PP)	*H*	0.05	0.44
9. Coefficient of dynamic friction (PP-Steel)	*I*	0.25	0.28

Note: poisson ratio of steel = 0.3, solid density of steel (kg/m^3) = 7800, and elastic modulus of steel (GPA) = 198

2. 6. 2. Plackett-Burmann Screening Experiment

The parameter screening stage evaluates main and interaction effects without considering the quadratic regression model. Plackett-Burmann (PB) method is commonly used for initial main effect analysis [16–18]. **Table 3** shows the 9-factor PB method with two levels each. The angles of repose results guide the selection of influential micro parameters through indirect measurement and significance analysis.

Table 3
Plackett-Burmann screening experiments through EDEM simulation software

No.	Factors									AOR (°)
	A	*B*	*C*	*D*	*E*	*F*	*G*	*H*	*I*	
1	0.41	1107	2	0.3	0.71	0.6	0.26	0.44	0.246	37.05
2	0.41	1107	1.3	0.97	0.55	0.1	0.26	0.44	0.28	15.77
3	0.36	1107	2	0.3	0.71	0.1	0.26	0.05	0.28	22.10
4	0.41	1107	1.3	0.97	0.71	0.1	0.3	0.05	0.246	19.42
5	0.41	889	1.3	0.3	0.71	0.6	0.3	0.05	0.28	29.53
6	0.41	889	2	0.97	0.55	0.6	0.26	0.05	0.246	27.29
7	0.36	889	1.3	0.3	0.55	0.1	0.26	0.05	0.246	21.94
8	0.36	1107	2	0.97	0.55	0.6	0.3	0.05	0.28	28.89
9	0.36	1107	1.3	0.3	0.55	0.6	0.3	0.44	0.246	39.27
10	0.36	889	2	0.97	0.71	0.1	0.3	0.44	0.246	16.61
11	0.41	889	2	0.3	0.55	0.1	0.3	0.44	0.28	22.78
12	0.36	889	1.3	0.97	0.71	0.6	0.26	0.44	0.28	25.16

2. 6. 3. Response surface implementation

Screening identifies influential factors used in response surface method (RSM), as shown in **Table 4**. RSM is employed to model the angle of repose based on micromechanical parameters [44]. It explores the quadratic relationship between parameters and angle of repose, as shown in **Fig. 6.**

Table 4
Central composite design (CCD) as face centered composite design type

Factors	Symbol	Level				
		–α	–1	0	1	α
Coefficient of static friction (PP-PP)	*F*	0.1	0.1	0.35	0.6	0.6
Coefficient of restitution (PP-PP)	*D*	0.3	0.3	0.635	0.97	0.97
Solid density (kg/m^3) (PP)	*B*	889	889	998	1107	1107

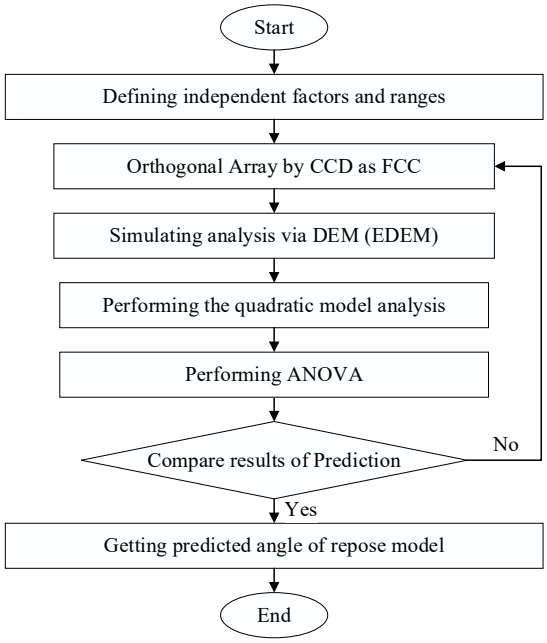

Fig. 6. Flow chart of Response surface methodology

2. 6. 4. Central composite design

The central composite design (CCD) designs experiments with all essential factors, followed by building the quadratic model. the central composite face-centered (CCF) design is used in this research, with 8 cube points, 6 center points, 6 axial points, and a radius of 1.0 (**Table 5**). AOR results evaluate the main factors and establish the quadratic equation.

Table 5
Design and results of central composite design (CCD) experiments

Run Order	Factors			AOR (°)
	F	*D*	*B*	
1	**2**	**3**	**4**	**5**
1	0.10	0.635	998	19.54
2	0.60	0.635	998	30.61
3	0.60	0.970	1107	25.28
4	0.35	0.635	998	27.37
5	0.60	0.970	889	23.80
6	0.35	0.635	998	30.11
7	0.35	0.635	998	30.11
8	0.35	0.635	889	24.54
9	0.35	0.970	998	21.89
10	0.10	0.970	889	16.43
11	0.60	0.300	1107	27.85
12	0.10	0.300	889	18.54

Continuation of Table 5

1	2	3	4	5
13	0.35	0.635	1107	26.07
14	0.35	0.635	998	30.11
15	0.10	0.970	1107	16.88
16	0.35	0.635	998	30.11
17	0.60	0.300	889	26.94
18	0.35	0.300	998	27.61
19	0.35	0.635	998	30.11
20	0.10	0.300	1107	20.93

2. 6. 5. Creating predicted model and analysis of variance (ANOVA)

Establish the quadratic model using DEM simulation results of AOR (17):

$$Y = A_0 + \sum_{i=1}^{k} A_i X_i + \sum_{i<j}^{k} A_{ij} X_i X_j + \sum_{i=1}^{k} A_{ii} X_i^2. \quad (17)$$

Y is the AOR response, X_i are variables, and A_0, A_i, A_{ii}, and A_{ij} are coefficients. ANOVA validates the AOR quadratic model's reliability, considering the influential parameters indicated in (17).

2. 6. 6. Optimal micro parameter for AOR model

Using RSM methodology, the fitness function is defined to seek suitable micro parameters based on the AOR laboratory test, shown in (18), (19):

$$\text{Find } X = [F, D, B], \quad (18)$$

$$\text{Maximum } Y(x), \quad (19)$$

$$\text{Subject to: } 0.1 \le F \le 0.6,$$

$$0.3 \le D \le 0.97,\ 889 \le B \le 1107\ (\text{kg/m}^3).$$

Fixed micro material parameters for the AOR test include: Poisson ratio of steel (0.3), Poisson ratio of polypropylene (0.36), Elastic modulus of steel (198 GPa), Elastic modulus of polypropylene (1.3 GPa), solid density of steel (7800 kg/m^3), coefficient of static friction (PP-Steel) (0.26), coefficient of dynamic friction (PP-PP) (0.05), coefficient of dynamic friction (PP-Steel) (0.246).

3. Result and discussions

Table 6 displays the measured axial dimension, equivalent diameter, particle mass, solid density, bulk density, and observed angle of repose of polypropylene particles. All values in **Table 5** have a COV below 10 %, indicating reliability [8]. The empirical angle of repose was 30.18°±0.51°, informing micromechanical material properties, while the solid density (910±0.889 kg/m^3) aligns with Fan et al's study [7].

Table 6

Physical properties and AOR of polypropylene measured in the laboratory

Axial dimension	Mean	Standard Deviation	(COV %)	Min	Max
Length (mm)	3.00	0.03	1.00	2.95	3.05
Width (mm)	3.01	0.01	1.11	2.95	3.05
Equivalent geometric particle diameter (mm)	3	0.011	0.37	2.98	3.02
Particle density (kg/m^3)	910	0.889	0.098	908	911
Angle of repose (degree)	30.18	0.51	1.67	29.25	30.86

Table 2 sets DEM micro properties with low and high levels. PB design (12 runs) is shown in **Table 3**. Steel properties are fixed. AOR results (16.43° to 30.61°) are dependent responses. **Table 7** concludes PB results, highlighting key parameters: PP-PP friction, restitution, and PP density. Their contribution exceeds 90 %.

Table 7

DEM parameters from the Plackett-Burmann design of experiment according to their order of the percent contribution

Parameters Symbol	Effect	Mean Square	Percent Contribution (%)	Contribution Order
A	–0.354	0.377	0.06	9
B	3.197	30.654	5.14	3
C	0.607	1.104	0.19	8
D	–6.589	130.232	21.84	2
E	–1.012	3.069	0.51	7
F	11.429	391.849	65.70	1
G	1.198	4.302	0.72	6
H	1.244	4.646	0.78	5
I	–2.896	25.16	4.22	4

Obtaining the coefficients of static friction (PP-PP, F), coefficient of restitution (PP-PP, D), and solid density (PP, B) constitutes the primary outcomes of the initial screening phase. The face-centered composite design (FCC) was employed to simulate AOR results, presented in **Table 5**. Subsequently, an analysis of variance (ANOVA) was conducted for the predictive AOR model of scaled-up particles, employing a backward elimination process detailed in **Table 8**. ANOVA significant terms, including «df» (degrees of freedom), «Adj SS» (adjusted sum of squares), «Adj Ms» (adjusted mean squares), «F-Value» (ratio of variation between sample means and within the samples), and «P-Value» (probability, less than 0.05), were investigated. **Table 8** reveals a coefficient of predicted determination (R-Sq (prediction)) exceeding 88%, indicating the model's high reliability. The backward elimination process highlights the prominent impact of static friction (PP-PP, F) and coefficient of restitution (PP-PP, D) on the scaled-up AOR phenomenon, including linear and square action impacts of both factors. Consequently, the response surface methodology generates a polynomial AOR equation for the main two factors, as expressed in Equation (20):

$$\mathrm{AOR}(^\circ) = 7.64 + 51.3F + 33.3D - 49.3F * F - 30.36D * D. \quad (20)$$

Table 8

ANOVA table for AOR model (after backward elimination)

Source	df	Adj SS	Adj MS	F-Value	P-Value
Model	4	376.878	94.219	29.33	0.000
Linear	2	208.513	104.256	32.45	0.000
F	1	177.611	177.611	55.28	0.000
D	1	30.902	30.902	9.62	0.007
Square	2	168.365	84.182	26.20	0.000
*F*F*	1	30.329	30.329	9.44	0.008
*D*D*	1	37.147	37.147	11.56	0.004
Error	15	48.190	3.213	–	–
Lack-of-Fit	10	41.952	4.195	–	–
Pure Error	5	6.238	1.248	–	–

Note: S = 1.79240, R-Sq = 88.66 %, R-Sq (adjust) = 85.64 %

By substituting (20) into (19) to form a fitness equation, the coefficient of static friction (PP-PP, F) and coefficient of restitution (PP-PP, D) were optimized using the RSM method. The optimal values for *F* and *D* were found to be 0.52 and 0.55, respectively. The other factors have been established at constant values: the Poisson ratio for steel set at 0.3, for polypropylene at 0.36, the elastic modulus for steel at 198 GPa, for polypropylene at 1.3 GPa, the solid density for steel at 7800 kg/m³, the coefficient of static friction (PP-Steel) at 0.26, the coefficient of dynamic friction (PP-PP) at 0.05, and the coefficient of dynamic friction (PP-Steel) at 0.246. When comparing the empirical laboratory AOR of 30.18° with the DEM simulation test results of 29.14° for 3-mm particles and 29.67° for 6-mm particles, with a fixed solid density of PP at 910 kg/m^3, the error percentages were 3.45 % and 1.69 % respectively. Future work involves validating these calibrated DEM parameters for various applications like hopper discharge and material handling equipment.

4. Conclusions

1. Establishing a scaled-up spheroid DEM polypropylene particle model (6-mm diameter) resulted in significant computational savings (71 %) compared to the unscaled particle in AOR simulations.

2. Using experimental designs and methodologies revealed that micromechanical properties (the coefficient of static friction (PP-PP, F) and coefficient of restitution (PP-PP, D) strongly influence scaled-up spheroid polypropylene particles.

3. A predictive equation successfully explained the relationship between DEM-predicted AOR, with a small error percentage (1.69 %) compared to laboratory tests.

Conflict of interest

The authors declare that they have no conflict of interest in relation to this research, whether financial, personal, authorship or otherwise, that could affect the research and its results presented in this paper.

Financing

The study was performed with financial support by Faculty of Engineering, King Mongkut's University of Technology North Bangkok. Contract no. ENG-NEW-65-37.

Data availability

Manuscript has no associated data.

Acknowledgements

This research was funded by Faculty of Engineering, King Mongkut's University of Technology North Bangkok. Contract no. ENG-NEW-65-37.

Use of artificial intelligence

The authors confirm that they did not use artificial intelligence technologies when creating the current work.

References

[1] Cundall, P. A., Strack, O. D. L. (1979). A discrete numerical model for granular assemblies. Géotechnique, 29 (1), 47–65. doi: https://doi.org/10.1680/geot.1979.29.1.47

[2] Grima, A., Wypych, P. (2010). Discrete element simulation of a conveyor impact-plate transfer: calibration, validation and scale-up. Australian Bulk Handling Review, 3, 64–72. Available at: https://www.researchgate.net/publication/288811749_Discrete_element_simulation_of_a_conveyor_impact-plate_transfer_Calibration_validation_and_scale-up

[3] Grima, A. P., Fraser, T., Hastie, D. B., Wypych, P. W. (2011). Discrete element modelling: Trouble-shooting and optimisation tool for chute design. Beltcon, 16, 1–26. Available at: https://ro.uow.edu.au/eispapers/882/

[4] Boac, J. M., Ambrose, R. P. K., Casada, M. E., Maghirang, R. G., Maier, D. E. (2014). Applications of Discrete Element Method in Modeling of Grain Postharvest Operations. Food Engineering Reviews, 6 (4), 128–149. doi: https://doi.org/10.1007/s12393-014-9090-y

[5] Chen, C., McDowell, G. R., Thom, N. H. (2012). Discrete element modelling of cyclic loads of geogrid-reinforced ballast under confined and unconfined conditions. Geotextiles and Geomembranes, 35, 76–86. doi: https://doi.org/10.1016/j.geotexmem.2012.07.004

[6] Van Lysebetten, G., Vervoort, A., Maertens, J., Huybrechts, N. (2014). Discrete element modeling for the study of the effect of soft inclusions on the behavior of soil mix material. Computers and Geotechnics, 55, 342–351. doi: https://doi.org/10.1016/j.compgeo.2013.09.023

[7] Fan, J., Zhang, S., Yao, B., Hao, Y., Zhu, X., Liu, X. (2021). Numerical simulation of the motion of polypropylene-particles in a horizontal straight pipe. Journal of Natural Gas Science and Engineering, 88, 103854. doi: https://doi.org/10.1016/j.jngse.2021.103854

[8] Zhang, S., Tekeste, M. Z., Li, Y., Gaul, A., Zhu, D., Liao, J. (2020). Scaled-up rice grain modelling for DEM calibration and the validation of hopper flow. Biosystems Engineering, 194, 196–212. doi: https://doi.org/10.1016/j.biosystemseng.2020.03.018

[9] Tijskens, E., Ramon, H., Van Besien, B., Vandewalle, S. (2006). Large Scale Dem Computation–Expectations and Recent Results. The 5th international conference for conveying and handling of particulate solids. Sorrento.

[10] Coetzee, C. J. (2016). Calibration of the discrete element method and the effect of particle shape. Powder Technology, 297, 50–70. doi: https://doi.org/10.1016/j.powtec.2016.04.003

[11] Beakawi Al-Hashemi, H. M., Baghabra Al-Amoudi, O. S. (2018). A review on the angle of repose of granular materials. Powder Technology, 330, 397–417. doi: https://doi.org/10.1016/j.powtec.2018.02.003

[12] Asaf, Z., Rubinstein, D., Shmulevich, I. (2007). Determination of discrete element model parameters required for soil tillage. Soil and Tillage Research, 92 (1-2), 227–242. doi: https://doi.org/10.1016/j.still.2006.03.006

[13] Chen, J., Gao, R., Liu, Y. (2019). Numerical Study of Particle Morphology Effect on the Angle of Repose for Coarse Assemblies Using DEM. Advances in Materials Science and Engineering, 2019, 1–15. doi: https://doi.org/10.1155/2019/8095267

[14] Li, C., Honeyands, T., O'Dea, D., Moreno-Atanasio, R. (2017). The angle of repose and size segregation of iron ore granules: DEM analysis and experimental investigation. Powder Technology, 320, 257–272. doi: https://doi.org/10.1016/j.powtec.2017.07.045

[15] Marigo, M., Stitt, E. H. (2015). Discrete Element Method (DEM) for Industrial Applications: Comments on Calibration and Validation for the Modelling of Cylindrical Pellets. KONA Powder and Particle Journal, 32, 236–252. doi: https://doi.org/10.14356/kona.2015016

[16] Zhu, J., Zou, M., Liu, Y., Gao, K., Su, B., Qi, Y. (2022). Measurement and calibration of DEM parameters of lunar soil simulant. Acta Astronautica, 191, 169–177. doi: https://doi.org/10.1016/j.actaastro.2021.11.009

[17] Xia, R., Li, B., Wang, X., Li, T., Yang, Z. (2019). Measurement and calibration of the discrete element parameters of wet bulk coal. Measurement, 142, 84–95. doi: https://doi.org/10.1016/j.measurement.2019.04.069

[18] Roessler, T., Katterfeld, A. (2019). DEM parameter calibration of cohesive bulk materials using a simple angle of repose test. Particuology, 45, 105–115. doi: https://doi.org/10.1016/j.partic.2018.08.005

[19] Pachón-Morales, J., Do, H., Colin, J., Puel, F., Perré, P., Schott, D. (2019). DEM modelling for flow of cohesive lignocellulosic biomass powders: Model calibration using bulk tests. Advanced Powder Technology, 30 (4), 732–750. doi: https://doi.org/10.1016/j.apt.2019.01.003

[20] El-Kassem, B., Salloum, N., Brinz, T., Heider, Y., Markert, B. (2020). A multivariate regression parametric study on DEM input parameters of free-flowing and cohesive powders with experimental data-based validation. Computational Particle Mechanics, 8 (1), 87–111. doi: https://doi.org/10.1007/s40571-020-00315-8

[21] Thakur, S. C., Ooi, J. Y., Ahmadian, H. (2016). Scaling of discrete element model parameters for cohesionless and cohesive solid. Powder Technology, 293, 130–137. doi: https://doi.org/10.1016/j.powtec.2015.05.051

[22] Roessler, T., Richter, C., Katterfeld, A., Will, F. (2019). Development of a standard calibration procedure for the DEM parameters of cohesionless bulk materials – part I: Solving the problem of ambiguous parameter combinations. Powder Technology, 343, 803–812. doi: https://doi.org/10.1016/j.powtec.2018.11.034

[23] Elskamp, F., Kruggel-Emden, H., Hennig, M., Teipel, U. (2017). A strategy to determine DEM parameters for spherical and non-spherical particles. Granular Matter, 19 (3). doi: https://doi.org/10.1007/s10035-017-0710-0

[24] Do, H. Q., Aragón, A. M., Schott, D. L. (2018). A calibration framework for discrete element model parameters using genetic algorithms. Advanced Powder Technology, 29 (6), 1393–1403. doi: https://doi.org/10.1016/j.apt.2018.03.001

[25] Mohajeri, M. J., Do, H. Q., Schott, D. L. (2020). DEM calibration of cohesive material in the ring shear test by applying a genetic algorithm framework. Advanced Powder Technology, 31 (5), 1838–1850. doi: https://doi.org/10.1016/j.apt.2020.02.019

[26] Ye, F., Wheeler, C., Chen, B., Hu, J., Chen, K., Chen, W. (2019). Calibration and verification of DEM parameters for dynamic particle flow conditions using a backpropagation neural network. Advanced Powder Technology, 30 (2), 292–301. doi: https://doi.org/10.1016/j.apt.2018.11.005

[27] Zhou, H., Hu, Z., Chen, J., Lv, X., Xie, N. (2018). Calibration of DEM models for irregular particles based on experimental design method and bulk experiments. Powder Technology, 332, 210–223. doi: https://doi.org/10.1016/j.powtec.2018.03.064

[28] Richter, C., Rößler, T., Kunze, G., Katterfeld, A., Will, F. (2020). Development of a standard calibration procedure for the DEM parameters of cohesionless bulk materials – Part II: Efficient optimization-based calibration. Powder Technology, 360, 967–976. doi: https://doi.org/10.1016/j.powtec.2019.10.052

[29] Westbrink, F., Elbel, A., Schwung, A., Ding, S. X. (2021). Optimization of DEM parameters using multi-objective reinforcement learning. Powder Technology, 379, 602–616. doi: https://doi.org/10.1016/j.powtec.2020.10.067

[30] Roessler, T., Katterfeld, A. (2018). Scaling of the angle of repose test and its influence on the calibration of DEM parameters using upscaled particles. Powder Technology, 330, 58–66. doi: https://doi.org/10.1016/j.powtec.2018.01.044

[31] Coetzee, C. J. (2019). Particle upscaling: Calibration and validation of the discrete element method. Powder Technology, 344, 487–503. doi: https://doi.org/10.1016/j.powtec.2018.12.022

[32] Lommen, S., Mohajeri, M., Lodewijks, G., Schott, D. (2019). DEM particle upscaling for large-scale bulk handling equipment and material interaction. Powder Technology, 352, 273–282. doi: https://doi.org/10.1016/j.powtec.2019.04.034

[33] Alsabri, A., Tahir, F., Al-Ghamdi, S. G. (2022). Environmental impacts of polypropylene (PP) production and prospects of its recycling in the GCC region. Materials Today: Proceedings, 56, 2245–2251. doi: https://doi.org/10.1016/j.matpr.2021.11.574

[34] D854-14. Standard Test Methods for Specific Gravity of Soil Solids by Water Pycnometer. ASTM. Available at: https://cdn.standards.iteh.ai/samples/87890/2765896e89474518be53b1b9507859b6/ASTM-D854-14.pdf

[35] Bande, Y. M., Adam, N. M., Azmi, Y., Jamarei, O. (2012). Moisture-dependent Physical and Compression Properties of Bitter Melon (Citrullus colocynthis lanatus) Seeds. International Journal of Agricultural Research, 7 (5), 243–254. doi: https://doi.org/10.3923/ijar.2012.243.254

[36] Bierwisch, C., Kraft, T., Riedel, H., Moseler, M. (2009). Three-dimensional discrete element models for the granular statics and dynamics of powders in cavity filling. Journal of the Mechanics and Physics of Solids, 57 (1), 10–31. doi: https://doi.org/10.1016/j.jmps.2008.10.006

[37] Bierwisch, C. S. (2009). Numerical Simulations of Granular Flow and Filling. Available at: https://d-nb.info/994194013/34

[38] Luo, K., Tan, J., Wang, Z., Fan, J. (2016). Particle-resolved direct numerical simulation of gas-solid dynamics in experimental fluidized beds. AIChE Journal, 62 (6), 1917–1932. doi: https://doi.org/10.1002/aic.15186

[39] Sturm, M., Wirtz, S., Scherer, V., Denecke, J. (2009). Coupled Discrete Element (DEM) – Continuous Fluid (CFD) Method for the Application of Pneumatic Conveyed Granular Media. Volume 4: Fluid-Structure Interaction. doi: https://doi.org/10.1115/pvp2009-77240

[40] Yurata, T., Gidaspow, D., Piumsomboon, P., Chalermsinsuwan, B. (2021). The importance of parameter-dependent coefficient of restitution in discrete element method simulations. Advanced Powder Technology, 32 (4), 1004–1012. doi: https://doi.org/10.1016/j.apt.2021.02.005

[41] Mesnier, A., Rouabah, M., Cogné, C., Peczalski, R., Vessot-Crastes, S., Vacus, P., Andrieu, J. (2019). Contact heating of bi-dispersed milli-beads in a rotary drum. Mechanical segregation impact on temperature distribution and on heating kinetic analyzed by DEM simulation. Powder Technology, 354, 240–246. doi: https://doi.org/10.1016/j.powtec.2019.05.059

[42] Olefins, I. (2014). Polymers. Typical Engineering Properties of Polypropylene.

[43] Zapata, N. C. R., Restrepo, J. M. V. (2008). Contact analysis of the solid polypropylene – AISI P20 mold steel tribosystem. Technical Papers, Regional Technical Conference – Society of Plastics Engineers, 4, 2214–2218.

[44] Xiao, J., Liu, G., Liu, J., Dai, J., Liu, H., Wang, P. (2019). Parameters of a discrete element ballasted bed model based on a response surface method. Journal of Zhejiang University-SCIENCE A, 20 (9), 685–700. doi: https://doi.org/10.1631/jzus.a1900133

Received date 21.06.2023
Accepted date 15.11.2023
Published date 30.11.2023

How to cite: *Sudsawat, S., Chongchitpaisan, P., Arunyanart, P. (2023). Calibrating polypropylene particle model parameters with upscaling and repose surface method. EUREKA: Physics and Engineering, 6, 34–46. doi: https://doi.org/10.21303/2461-4262.2023.002968*